Applied Physics A (2023) 129:171
https://doi.org/10.1007/s00339-023-06458-8

Applied Physics A
Materials Science & Processing

Enhanced temperature sensing performance of Er^{3+}, Yb^{3+}: PLZT ceramic based on emissions of Stark sublevels

Shaobo Yao[1] · Shaozhen Lv[1] · Zhuohong Feng[2]

Received: 11 October 2022 / Accepted: 25 January 2023 / Published online: 5 February 2023

Abstract

In this study, the temperature sensing behaviors of emissions of Stark sublevels in Er^{3+}/Yb^{3+} codoped lead lanthanum zirconate titanate (PLZT) transparent ceramic were examined. Based on the temperature-dependent upconversion fluorescence spectra excited by 980 nm, the emission intensities of the Stark sublevels $^2H_{11/2(1,2)}$, $^4S_{3/2(1,2)}$, and $^4F_{9/2(1,2,3)}$ were obtained upon increasing the temperature from 160 to 320 K. All the transitions present strong temperature dependence under the competitive effects of thermal excitation and nonradiative relaxation. The optical temperature sensing properties of $^2H_{11/2}/^4S_{3/2(1)}$, $^2H_{11/2}/^4S_{3/2(2)}$, $^2H_{11/2}/^4F_{9/2(1)}$, $^2H_{11/2}/^4F_{9/2(2)}$, and $^2H_{11/2}/^4F_{9/2(3)}$ were investigated using the fluorescence intensity ratio (FIR) technique. The largest absolute sensitivity S_a of 142.4×10^{-4} K^{-1} was obtained based on the FIRs of $^2H_{11/2}/^4F_{9/2(1)}$ at 320 K, which is approximately 26 times larger than that of traditionally used thermal coupled levels $^2H_{11/2}/^4S_{3/2}$ in the considered sample. In contrast, the maximum relative sensitivity S_r was 2.21% K^{-1} at 203 K. A comparison of these results with those of other Er^{3+}/Yb^{3+} codoped materials reveals that Er^{3+}/Yb^{3+}: PLZT ceramics are a promising thermometer material at low temperatures. Applying FIRs based on the photoluminescence of Stark sublevels is a practical approach to achieving greater thermometric efficiency.

Keywords Temperature sensing · Enhanced temperature sensitivity · Fluorescence intensity ratio · Emissions of Stark sublevel · Er^{3+}/Yb^{3+} codoped PLZT transparent ceramic

1 Introduction

Temperature measurements with high sensitivity and accuracy have become vital in many fields including daily life, industrial production, and scientific research [1–3]. In recent years, optical thermometry has attracted considerable interest owing to its noncontact characteristics, better accuracy, higher reliability, and broader applications as compared with traditional contact thermometers [4–7]. It can be used in harsh environments, such as those with high temperatures and pressure, and corrosive areas [8]. Among several optical thermometry methods, the fluorescence intensity ratio (FIR) based on the thermal coupled level transitions of rare-earth ions is believed to be the most promising and reliable for temperature measurements [9–13].

Upconversion luminescence materials codoped with Er^{3+} and Yb^{3+} ions have been studied [14–16]. As one of the most widely used activators, Er^{3+} ions have typical thermal coupled levels (TCLs) of $^2H_{11/2}$ and $^4S_{3/2}$, which relative emission intensity presents strong temperature dependence, and were applied to temperature sensing [17, 18]. By codoping Yb^{3+} ions as sensitizers, Er^{3+}/Yb^{3+} doped materials can be effectively pumped by a commercial 980 nm laser diode and thus strengthen the intensity of upconversion luminescence [15]. This type of photoluminescence also has some other attractive advantages. In the previous published literatures [19], the absorption and scattering coefficients of human skin, subcutaneous adipose tissue and mucous in the wavelength range from 400 to 2000 nm have been studied. 980 nm have pretty low absorption and scattering coefficient, relative long tissue penetrate distance and non-biological toxicity, which make it possible to be used in biomedicine field. Some literature have reported the UC thermometer

Shaobo Yao, Shaozhen Lv have contributed equally to this work.

✉ Zhuohong Feng
lvshaozhen2014@163.com

[1] School of Electronic, Electrical Engineering and Physics, Fujian University of Technology, Fuzhou 350117, China

[2] College of Physics and Energy, Fujian Normal University, Fuzhou 350117, China

using FIR method for biomedical application [20–22]. For those broader application and attracted features, searching different optical temperature sensor materials can provide a more favorable opportunity to select different sensing functions according to the practical requirement.

The luminescence intensity and sensor sensitivity are essential for the practical application. Searching TCLs with larger energy gaps have been proposed for developing efficient methods with greater sensitivity [23]. In our previous work, the $^2H_{11/2}$, $^4S_{3/2,}$ and $^4F_{9/2}$ levels were shown to be thermal coupled multi-levels (TCMLs). The temperature sensitivity of FIR of $^2H_{11/2}$/$^4F_{9/2}$ is approximately 4 times larger than that of $^2H_{11/2}$/$^4S_{3/2}$ in Er^{3+}/Yb^{3+} codoped PLZT ceramics [24]. To investigate the possibility of further enhancing the temperature sensitivity, we studied the thermal luminescence characteristics of Stark sublevels in the same sample. Stark sublevels can also be considered as TCLs for the small level gap. The emissions of small level gaps were studied as another valid strategy for improving sensitivity [25–27]. For instance, Liu reported the maximum absolute sensitivity of $^2H_{11/2}$ to $^4S_{3/2(1)}$ levels as about onefold higher than that of traditionally used TCLs $^2H_{11/2}$/$^4S_{3/2}$ in Er^{3+}/Yb^{3+} codoped $Ba_3Y_4O_9$ [28]. In addition, the sensitivity based on FIRs of $^2H_{11/2}$ to $^4S_{3/2(1)}$ or $^2H_{11/2}$ to $^4S_{3/2(2)}$ is almost twice enhanced in Er^{3+}/Yb^{3+} codoped $Gd_2(WO_4)_3$ [14]. As a traditional and widely studied material, PLZT transparent ceramic was selected as the host. The lower phonon energy (750 cm^{-1}) and higher refraction index (2.401) of PLZT can result in higher transition probabilities than other rare-earth-doped host like $LiNbO_3$ [29], and ceramics usually have better mechanical, thermal, and chemical resistances [29, 30].

In this study, the luminescence properties of the Stark sublevels of the $^2H_{11/2}$, $^4S_{3/2}$, and $^4F_{9/2}$ levels in Er^{3+}/Yb^{3+} codoped PLZT transparent ceramic were investigated based on the upconversion spectra under the 980 nm excitation, and the temperature-dependent emission intensities of the Stark sublevels were studied in the temperature range from 160 to 320 K. The FIRs of the Stark sublevels' emissions were studied for the enhancement of temperature sensing sensitivity. Moreover, the results of this study are helpful for better understanding the temperature characteristics of the Stark sublevels' relative intensities.

2 Experimental

The Er^{3+}/Yb^{3+} codoped PLZT transparent ceramic was fabricated by the mixed-oxide method at Boston Applied Technologies Inc., USA. Then, a 3 mm × 3 mm × 2 mm sample was cut from the bulk ceramic and polished. This sample consists of 65 mol% lead zirconate plus 35 mol% lead titanate and 8 mol% lanthanum in the form of La_2O_3, i.e., PLZT(8/65/35), to which 0.5 mol% Er^{3+} ions in the form of Er_2O_3 and 2.5 mol% Yb^{3+} ions in the form of Yb_2O_3 had been added. The origins of components were PbO, ZrO_2, La_2O_3, TiO_2, Er_2O_3 and Yb_2O_3, respectively. PbO was purchased from Hammond Lead Products, with purity of 99.98%. All other oxides were purchased from Fisher Scientific have purity 99.85% or higher. A typical sintering process of the ceramic was published elsewhere [31]. By the inductively coupled plasma-atomic emission spectrometry (ICP-AES), the quantities of Er^{3+} and Yb^{3+} ions in the sample were determined to be 1.39×10^{20} ions/cm^3 and 6.70×10^{20} ions/cm^3, respectively. The upconversion spectrum and temperature fluorescence spectra were measured by a steady-state/lifetime spectrofluorometer (FLS 920, Edinburgh Instruments) excited by a 980 nm laser diode with emission slit size 0.5 nm, power 1000 mw, detection sensitivity (≤ 50 cps), integration time of 0.1 s and step of 0.5 nm, in here, the temperature of sample was real-time control by temperature control components of spectrofluorometer FLS 920 with 0.1 °C accuracy.

3 Results and discussion

The temperature-dependent upconversion spectra of Er^{3+}/Yb^{3+}: PLZT ceramic in the temperature range from 160 to 320 K were measured under 980 nm excitation (Fig. 1). The $^2H_{11/2}$ and $^4S_{3/2}$ levels are split into two sublevels $^2H_{11/2(1)}$ and $^2H_{11/2(2)}$ and $^4S_{3/2(1)}$ and $^4S_{3/2(2)}$, and the $^4F_{9/2}$ level is split into three sublevels: $^4F_{9/2(1)}$, $^4F_{9/2(2),}$ and $^4F_{9/2(3)}$. Seven luminescence band peaks at 527 nm, 539 nm, 551 nm, 564 nm, 655 nm, 665 nm, and 680 nm were found according to the transitions from the $^2H_{11/2(1)}$, $^2H_{11/2(2)}$, $^4S_{3/2(1)}$, $^4S_{3/2(2)}$, $^4F_{9/2(1)}$, $^4F_{9/2(2)}$, and $^4F_{9/2(3)}$ levels, respectively, to the ground level $^4I_{15/2}$.

Figure 2 shows the energy level scheme and relevant radiative transitions in this material. PLZT($Pb_{1-x}La_x(Zr_yT$

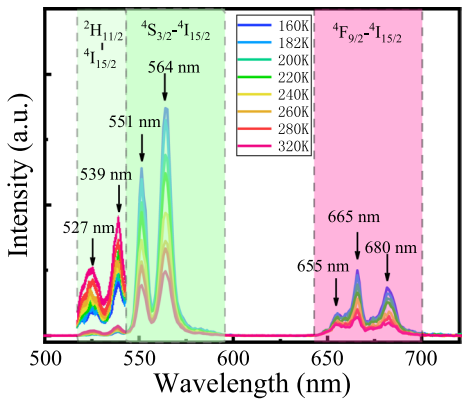

Fig. 1 Temperature-dependent upconversion spectra of the Er^{3+}/Yb^{3+}: PLZT ceramic excited by 980 nm in the 160–320 K temperature range

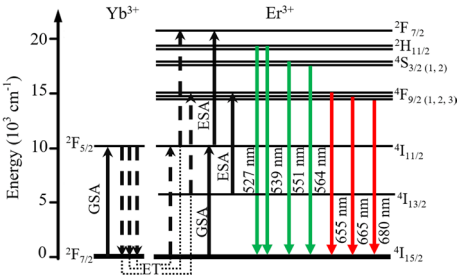

Fig. 2 Schematic energy level diagram and transitions mechanisms of Er^{3+}/Yb^{3+}: PLZT ceramic

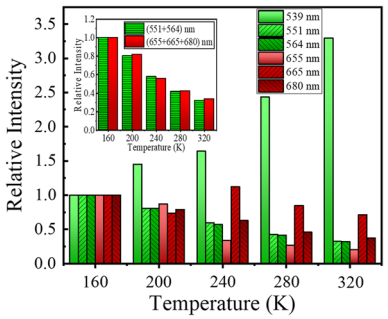

Fig. 3 Relative luminescence integrated intensities of the emissions of sublevels at different temperatures ranging from 160 to 320 K

$i_{1-y})_{1-x}O_3$) have the perovskite structure with the formation of ABO_3, in which La substitutes for Pb^{2+} in the A-site and the B-site vacancies are created for electric balance. When rare earth ion doped in PLZT, Re^{3+} ion (Er^{3+},Yb^{3+}) will occupy the position of La^{3+} for their similar ionic radii and charge characters. Since in our sample, the concentration of Yb^{3+} is around five times larger than Er^{3+} ion and Yb^{3+} has a much larger absorption cross-section around 980 nm than that of Er^{3+} ion, which we have discussed in our previous work for the same sample, the 980 nm pumping is mainly absorbed by the Yb^{3+} ion [31]. Thus, the mechanism for the up-conversion emission can be explained as follows.

After absorbing the energy of incident light, the Yb^{3+} ions can be excited from the ground level $^2F_{7/2}$ to upper levels $^2F_{5/2}$. Due to the close energy level of $^2F_{5/2}$ and $^4I_{11/2}$, the energy transfer process effectively occur between Yb^{3+} and Er^{3+} ion, that is $^2F_{5/2}(Yb^{3+})+{}^4I_{15/2}(Er^{3+})\rightarrow{}^2F_{7/2}(Yb^{3+})+{}^4I_{11/2}(Er^{3+})$. Meantime, the Er^{3+} ion in its ground level can also absorb the pumping energy and excited to$^4I_{11/2}$ level. Then, the ions accumulate in Er^{3+}:$^4I_{11/2}$ level absorb other photon energy and excited to upper $^4F_{7/2}$ level. And Yb^{3+} ion can also absorb a second photon and transfer its energy to Er^{3+} ion by $^2F_{5/2}(Yb^{3+})+{}^4I_{11/2}(Er^{3+})\rightarrow{}^2F_{7/2}(Yb^{3+})+{}^4F_{7/2}(Er^{3+})$,which also contribute to the accumulation of $^4F_{7/2}$ level. Ions in $^4F_{7/2}$ level rapidly relax to the sublevels of $^2H_{11/2}$ and $^4S_{3/2}$ level, and then some of them radiatively relax to the ground level and generate green emission. The other ions relax to $^4F_{9/2}$ level. Besides, the accumulation of $^4F_{9/2}$ level also comes from the excited level $^4I_{13/2}$ photon absorption and the energy transfer process: $^2F_{5/2}(Yb^{3+})+{}^4I_{13/2}(Er^{3+})\rightarrow{}^2F_{7/2}(Yb^{3+})+{}^4F_{9/2}(Er^{3+})$. Finally, the ions in $^4F_{9/2}$ sublevels decay to the ground level and generate red emission. The cross relaxation between Er^{3+} ions ($^4I_{11/2}+{}^4I_{11/2}\rightarrow{}^4I_{15/2}+{}^4F_{7/2}$, $^4I_{11/2}+{}^4I_{13/2}\rightarrow{}^4I_{15/2}+{}^4F_{9/2}$) also help for the population accumulation of $^4F_{7/2}$ and $^4F_{9/2}$ level, which can't be neglected in the sample with Er^{3+} concentration larger than 0.5 mol% [32]. But since those cross relaxation often obviously take place in the more heavily doped materials [33], and the Er^{3+} ion concentration is pretty low in our sample, those cross relaxation may be less due to the competitive mechanism.

Figure 1 also provides the temperature-dependent properties of the upconversion emissions from 160 to 320 K. The positions of the emission peaks barely changed with the increase of temperature, while the intensities changed remarkably. To further investigate the influence of temperature on the luminescence intensity of each transition, the relative integrated intensities normalized to the intensities at 160 K were calculated (Fig. 3). Here, the intensities of $^2H_{11/2\ (1)}$ and $^2H_{11/2\ (2)}$ were summed to be 539 nm to reduce calculation errors due to weaker luminescence. Figure 3 shows that all the transitions show strong temperature dependence. With the increase of temperature, the fluorescence integrated intensity of 539 nm evidently increased, while that of I_s (the sum of intensities of 551 nm and 564 nm, $^4S_{3/2(1,\ 2)}\rightarrow{}^4I_{15/2}$) and I_F (the sum of intensities of 655 nm, 665 nm, and 680 nm, $^4F_{9/2(1,\ 2,\ 3)}\rightarrow{}^4I_{15/2}$) uniformly decreased from 160 to 320 K, as shown in the inset of Fig. 3. This was because of thermal excitation between the TCLs [24].

In the green emission of I_s, the intensities of 551 nm and 564 nm have the same decreasing trend with temperature, and the ions in the $^4S_{3/2(1)}$ and $^4S_{3/2(2)}$ levels were thermally excited to the $^2H_{11/2}$ level simultaneously because of their similar small energy gap. However, in the red emission of I_F, the intensity of 665 nm abnormally increases at 240 K. The abnormal increase can be attributed to the competitive effects of thermal excitation and nonradiative relaxation. The $^4F_{9/2(2)}$ level is laying in the gap of the $^4F_{9/2(1)}$ and $^4F_{9/2(3)}$ levels. With the increase of temperature, the population of the $^4F_{9/2(2)}$ is benefited by the nonradiative relaxation of the $^4F_{9/2(1)}$ level and thermal excitation of the $^4F_{9/2(3)}$ level as well as expended by the nonradiative relaxation to $^4F_{9/2(3)}$ and thermal excitation to $^4F_{9/2(1)}$ level. The $^4F_{9/2(1)}$ level with higher energy provides a thermal excitation barrier for transitions from the $^4F_{9/2(2)}$ to the $^4S_{3/2}$ level. Therefore, the intensity of 665 nm increases from 160 to 240 K. With a further increase in temperature, the efficiency of thermal

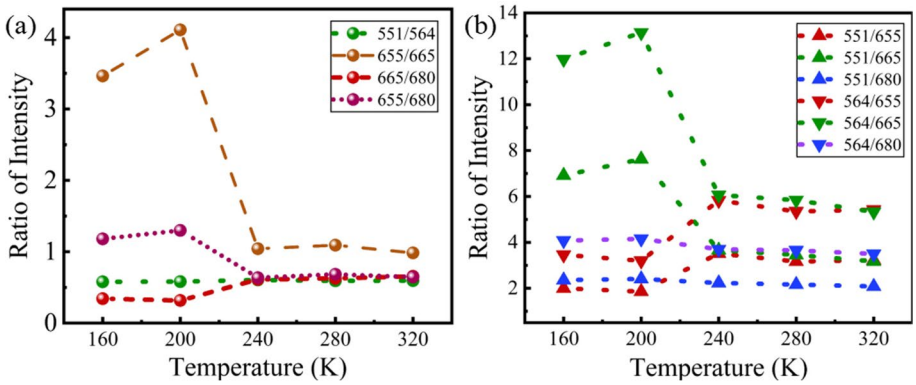

Fig. 4 **a** FIRs of the emissions of the sublevels of the $^4S_{3/2}$ level or $^4F_{9/2}$ levels, **b** FIRs of emissions the of sublevels of the $^4S_{3/2}$ level and $^4F_{9/2}$ levels

excitation increases, and the intensity of 665 nm decreases. Comparing the variation characteristics of intensities of 655, 665, and 680 nm from 240 to 320 K, thermal excitation was more dominant above 240 K, and their intensities show a similar decreasing trend with increasing temperature.

To elucidate the temperature sensing properties of TCMLs, the ratios between the emissions of the $^4S_{3/2(1,\ 2)}$ and $^4F_{9/2(1,\ 2,\ 3)}$ levels were examined (Fig. 4). The values of different ratios in Fig. 4 do not change above 240 K, indicating that the ions in the $^4S_{3/2(1,\ 2)}$ and $^4F_{9/2(1,\ 2,\ 3)}$ levels are thermally excited to the $^2H_{11/2}$ level simultaneously. For the intensities of 655 nm or 665 nm, the ratios change dramatically under 240 K, which is because of thermal excitation and nonradiative relaxation for lower temperatures.

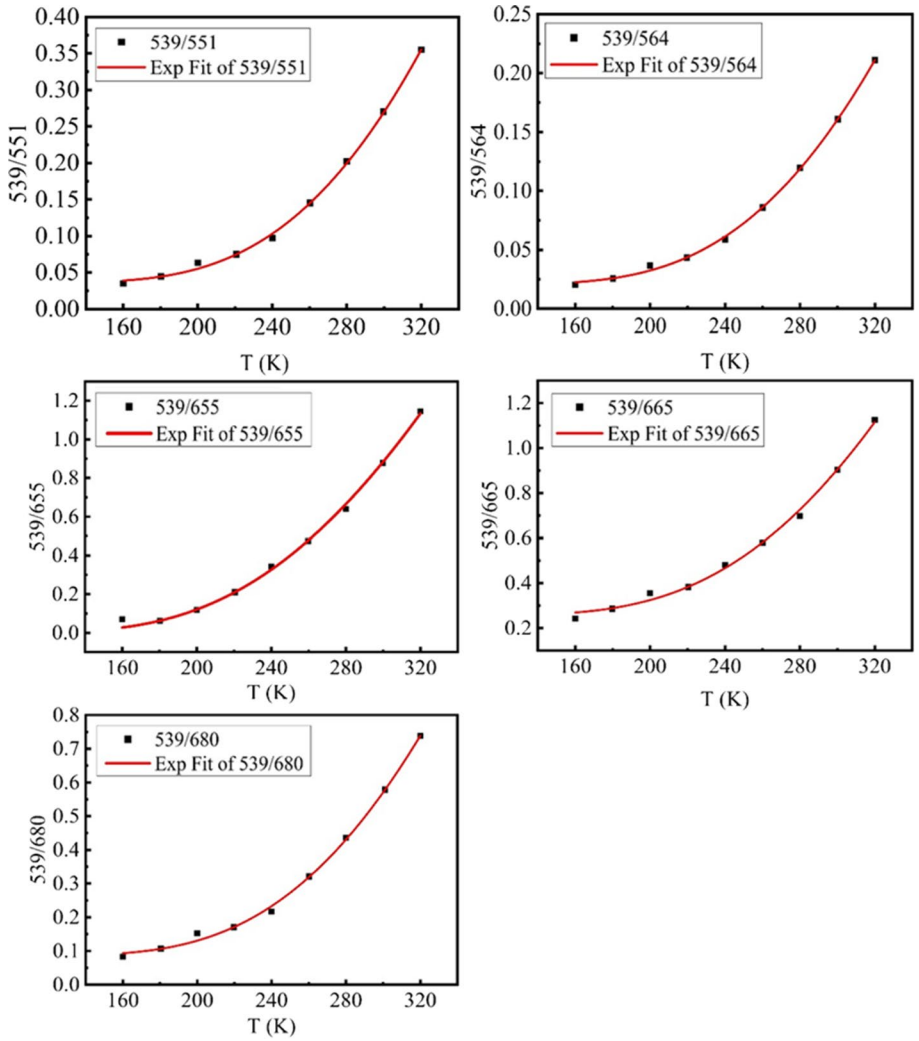

Fig. 5 Temperature-dependent luminescent behaviors of 539/551, 539/564, 539/655, 539/665, and 539/680 as a function of temperature

However, the ratios of 551/564, 551/680, and 564/680 remain for the entire experimental temperature range. The most important deduction is that for the lowest level and intermediate ladder level, the relative populations of $^4S_{3/2(1,2)}$ to $^4F_{9/2(1,2,3)}$ should not follow the Boltzmann distribution, and the FIRs of the levels cannot be used for temperature sensing in this sample.

The experimental data of 539/551, 539/564, 539/655, 539/665, and 539/680 were obtained and depicted in Fig. 5. The FIRs of five pairs were fitted with $A\exp(-B/T)+C$ [24]. Here, A is determined by the degeneracy, the emission cross-section, and the angular frequency of two levels, B is determined by $\Delta E/k_B$, and C is introduced to simplify the equation [34]. The fitting formula are listed in Table 1. The theoretical curves match the experimental results well. The values of B in Table 1 are similar and between the actual $\Delta E/k_B$ of $^2H_{11/2}/^4S_{3/2}$ and $^2H_{11/2}/^4F_{9/2}$. The intermediate ladder level $^4S_{3/2}$ can effectively reduce the transition interval limit of TCLs [24]. Meanwhile, the values of B are different owing to laser power fluctuations, the host matrix's absorption, and the thermal effect of nonradiative relaxation [35].

The absolute sensitivity S_a and relative sensitivity S_r of FIRs were obtained, as shown in Fig. 6. The S_a of the five pairs increase nonlinearly with increasing temperature, among which the S_a of 539/655 increases for the entire temperature range and are maximized at 320 K as 142.4×10^{-4} K^{-1}. Meanwhile, S_r of 539/655 is superior to those of other pairs, which is greater than 1.5% K^{-1} in the temperature range from 170 to 290 K with maximum value of 2.21% K^{-1} at 203 K. The maximum temperature sensitivities of five pairs are listed in Table 2. The FIRs of Stark sublevels significantly enhanced the absolute sensitivity, and the maximum S_a is approximately 26 times larger than that of traditionally used $^2H_{11/2}/^4S_{3/2}$ levels, which is also larger than that of other Er^{3+} doped hosts such as Al_2O_3, $NaYF_4$, YAG, Gd_2O_3, and $CaMoO_4$ [36–43]. The enhanced sensitivity is attributed to the energy gaps of corresponding thermal levels and the relative radiative transition probabilities [14]. The absolute sensitivity S_a of the Er^{3+}/Yb^{3+}: PLZT ceramic was compared with other Er^{3+}/Yb^{3+} codoped materials based on the FIRs of Stark sublevels, as listed in Table 3. The maximum S_a of the Er^{3+}/Yb^{3+}: PLZT ceramics is higher than that of most Er^{3+}/Yb^{3+} codoped phosphors. Thus, these Er^{3+}/Yb^{3+}: PLZT ceramics are promising materials for use as optical thermometers for temperatures higher than 160 K because of their enhanced temperature sensitivity.

Table 1 FIRs of five pairs fitted with the Boltzmann distribution

Pairs	Fitting formula	R^2
539/551	$34.45\times\exp(-1498/T)+0.03598$	0.997
539/564	$19.73\times\exp(-1485/T)+0.02067$	0.998
539/655	$47.39\times\exp(-1194/T)+0.00008$	0.995
539/665	$58.85\times\exp(-1353/T)+0.2569$	0.990
539/680	$56.90\times\exp(-1430/T)+0.08573$	0.994

Table 2 Temperature sensitivities of FIRs of the emissions of Er^{3+}/Yb^{3+} codoped PLZT ceramic

Pair for levels	S_a-max (10^{-4} K^{-1})	S_r-max (% K^{-1})	References
$^2H_{11/2}/^4S_{3/2}$	5.909 (320)	4.04 (140 K)	[19]
$^2H_{11/2}/^4F_{9/2}$	21.84 (320)	6.12 (140 K)	[19]
$^2H_{11/2}/^4S_{3/2\,(1)}$	46.70 (320)	1.70 (244 K)	This work
$^2H_{11/2}/^4S_{3/2\,(2)}$	27.62 (320)	1.71 (242 K)	
$^2H_{11/2}/^4F_{9/2\,(1)}$	142.4 (320)	2.21 (203 K)	
$^2H_{11/2}/^4F_{9/2\,(2)}$	113.4 (320)	1.12 (270 K)	
$^2H_{11/2}/^4F_{9/2\,(3)}$	91.07 (320)	1.57 (244 K)	

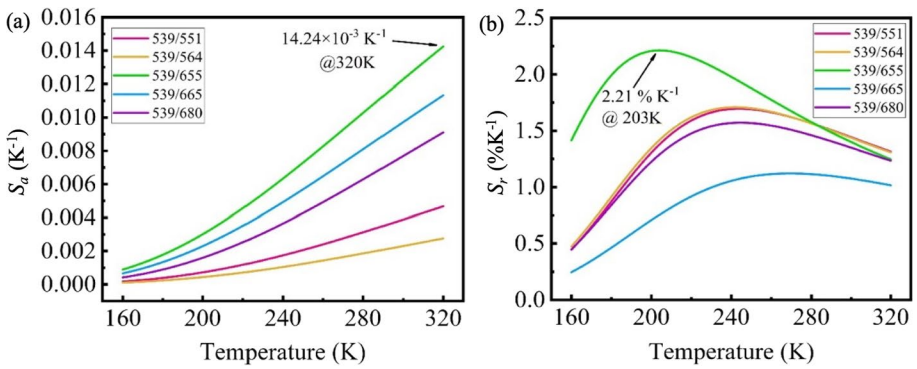

Fig. 6 **a** Absolute temperature sensitivity S_a and **b** relative temperature sensitivity S_r of the FIRs of five pairs

Table 3 Maximum absolute temperature sensitivities of some Er^{3+}/Yb^{3+} codoped hosts based on FIRs of Stark sublevels

Host	Transition	S_a -max (10^{-4} K^{-1})	S_r -max (% K^{-1})	Temperature range (K)	References
PLZT	$^2H_{11/2}/^4F_{9/2(1)}$	142.4 (320 K)	2.21 (203 K)	160–320	This work
$Gd_2(WO_4)_3$	$^2H_{11/2}/^4S_{3/2(2)}$	165 (395)	0.91 (296 K)	296–620	[14]
$Ba_3Y_4O_9$	$^2H_{11/2}/^4S_{3/2(1)}$	88.3 (523 K)	1.21 (298 K)	298–573	[28]
$CaO–Y_2O_3$	$^4F_{9/2(1)}/^4F_{9/2(3)}$	6.5 (298 K)	0.667 (298 K)	298–573	[44]
$Sr_3(PO_4)_2$	$^2H_{11/2(1)}/^4S_{3/2(2)}$	91 (623 K)	0.81 (350 K)	303–623	[45]
LiCaLa $(W_{0.1}Mo_{0.9}O_4)_3$	$^2H_{11/2}/^4S_{3/2(1)}$	134 (653 K)	4.34 (163 K)	163–653	[18]
Gd_2O_3	$^2H_{11/2(1)}/^4S_{3/2(2)}$	127 (574 K)	1.40 (301 K)	301–575	[46]
Gd_2O_3	$^2H_{11/2}/^4S_{3/2(2)}$	125 (478 K)	1.08 (298 K)	298–578	[47]
TiO_2	$^2H_{11/2}/^4S_{3/2}$	76.7 (307 K)	0.69 (307 K)	307–673 K	[48]

4 Conclusion

The temperature-dependent emissions of the Stark sublevels of Er^{3+}/Yb^{3+} codoped PLZT transparent ceramic were studied within 160–320 K based on upconversion fluorescence spectra under 980 nm excitation. Notably, $^2H_{11/2}$ and $^4S_{3/2}$ level are split into two sublevels as $^2H_{11/2(1,\ 2)}$ and $^4S_{3/2(1,\ 2)}$, and $^4F_{9/2}$ level is split into three sublevels as $^4F_{9/2(1,\ 2,\ 3)}$. All the level transitions have strong temperature dependence. The temperature characteristics of the emissions of the Stark sublevels were studied, and we found that the relative intensities of the lower level $^4F_{9/2}$ and intermediate step level $^4S_{3/2}$ in TCMLs cannot be used for temperature sensing. Hence, the FIRs of 539/551, 539/564, 539/655, 539/665, and 539/680 were studied and theoretically fitted for temperature sensing. The maximum values of absolute sensitivity S_a and relative sensitivity S_r were obtained as 142.4×10^{-4} K^{-1} at 320 K and 2.21% K^{-1} at 203 K, respectively. The S_a was enhanced 26 times, while the S_r is greater than 1.5% K^{-1} in the temperature range from 170 to 290 K. A comparison with other Er^{3+}/Yb^{3+} codoped materials shows that Er^{3+}/Yb^{3+}: PLZT ceramics are a promising thermometer material for temperatures greater than 160 K. Meanwhile, the application of FIRs based on the emissions of Stark sublevels might enhance temperature sensing performance.

Acknowledgements This work was supported by National Natural Science Foundation of China (No. 11204039 and 51202033); Natural Science Foundation of Fujian Province of China (No. 2022J01951, No. 2021J01183, 2020J01194, 2020J01190 and 2019J01283); Nature fund Projects of Education Department of Fujian Province (JA15338, JA15354).

Availability of data and materials All relevant data are within the paper and the data are available from the corresponding author on reasonable request.

Declarations

Conflict of interest The authors declare that they have no known competing financial interests or personal relationships that could have appeared to influence the work reported in this paper.

References

1. M.W. Khalid, C. Whitehouse, R. Ahmed, M.U. Hassan, H. Butt, Adv. Opt. Mater. **7**, 1801013 (2019)
2. X. Tian, T. Zhou, J. Wen, Z. Chen, C. Ji, Z. Huang, S. Lian, X. Liu, H. Peng, C. Li, J. Li, J. Hu, Y. Peng, Mater. Res. Bull. **129**, 110882 (2020)
3. J.R. Macairan, D.B. Jaunky, A. Piekny, R. Naccache, Nanoscale Adv. **1**, 105–113 (2019)
4. J. Zhou, Q. Liu, W. Feng, Y. Sun, F. Li, Chem. Rev. **115**, 395–465 (2015)
5. M.M.A. Mazza, F.M. Raymo, J. Mater. Chem. C **7**, 5333 (2019)
6. F.F. Hu, Y.C. Jiang, Y.H. Chen, R.F. Wei, H. Guo, C.K. Duan, J. Alloys Compd. **867**, 159160 (2021)
7. Y.H. Chen, J. Chen, Y. Tong, W.N. Zhang, X.S. Peng, H. Guo, D. Huang, J. Rare Earths **39**, 1512 (2021)
8. H. Zhang, S. Zhao, X. Wang, X. Ren et al., J. Mater. Chem. C **7**, 15007–15013 (2019)
9. S. Zheng, W. Chen, D. Tan, J. Zhou, Q. Guo et al., Nanoscale Adv. **6**, 5675–5679 (2014)
10. X. Xu, Z. Wang, P. Lei, Y. Yu, S. Yao et al., ACS Appl. Mater. Interfaces **7**, 20813–20819 (2015)
11. X. Yang, S.P. Lin, D.C. Ma, S.W. Long et al., Ceram. Int. **46**, 1178–1182 (2020)
12. E. Maurice, G. Monnom, D. Ostrowsky, G. Baxter, J. Light. Technol. **13**, 1349–1353 (1995)
13. A. Pandey, V. K. Rai, in Rare earth doped materials for temperature sensors, ed. by Y. Dwivedi, S. B. Rai, J. P. Singh (Nova Publisher, USA, Chapter 11, 2014), pp. 279–292
14. H. Lu, R. Meng, H. Hao, Y. Bai, Y. Gao, Y. Song et al., RSC Adv. **6**, 57667–57671 (2016)
15. L. Xu, J. Liu, L. Pei, Y. Xu, Z. Xia, J. Mater. Chem. C **7**, 6112–6119 (2019)
16. Y. Zhao, X.S. Wang, R. Hu, Y. Zhang, Y.X. Li, X. Yao, Mater. Res. Bull. **131**, 110959 (2020)

17. X. Wang, Q. Liu, Y. Bu, C. Liu, T. Liu, X.H. Yan, RSC Adv. **5**, 86219–86236 (2015)
18. Y. Zhao, X. Wang, Y. Zhang, Y. Li, X. Yao, J. Alloys Compd. **817**, 152691 (2020)
19. A.N. Bashkatov et al., J. Phys. D: Appl. Phys. **38**, 2543 (2005)
20. Y. Zhang, S. Xu, X. Li, J. Zhang, J. Sun, H. Xia, R. Hua, B. Chen, Mater. Res. Bull. **114**, 148–155 (2019)
21. X. Zhu, J. Li, X. Qiu, W. Feng, F. Li, Nat. Commun. **9**, 2176 (2018)
22. C. Duan, L. Liang, L. Li, R. Zhang, Z. Xu, J. Mater. Chem. B **6**, 192–209 (2018)
23. Y. Cheng, Y. Gao, H. Lin, F. Huang, Y. Wang, J. Mater. Chem. C **6**, 7462–7478 (2018)
24. Z. Feng, L. Lin, Z. Wang, Z. Zheng, Opt. Commun. **399**, 40–44 (2017)
25. O.A. Savchuk, J.J. Carvajal, M.C. Pujol et al., J. Phys. Chem. C **119**, 18546–18558 (2015)
26. N. Dong, M. Pedroni, F. Piccinelli, G. Conti, A. Sbarbati et al., ACS Nano **5**, 8665–8671 (2011)
27. A. Dwivedi, K. Mishra, S. Rai, J. Phys. D Appl. Phys. **48**, 435103 (2015)
28. S. Liu, H. Ming, J. Cui, S. Liu, W. You et al., J. Phys. Chem. C **122**, 16289–16303 (2018)
29. A.S.S. De Camargo, L.A.O. De Nunes, I.A. Santos et al., J. Appl. Phys. **95**, 2135 (2004)
30. G.H. Haertling, Ferroelectrics **75**, 25–55 (1987)
31. Z. Zheng, X. Li, J. Liu, Z. Feng, B. Li, J. Yang, K. Li, H. Jiang, X. Chen, J. Xie, H. Ming, Phys. B **403**, 44–49 (2008)
32. J.H. Yang, L. Wen, S.X. Dai, L.L. Hu, Z.H. Jiang, Chin. Opt. Lett. **1**, 611 (2003)
33. W.Q. Shi, M. Bass, M. Birnbaum, J. Opt. Soc. Am. B. **7**, 1456–1462 (1990)
34. Z. Feng, L. Lin, Z. Wang, Z. Zheng, J. Lumin. **221**, 117005 (2020)
35. X. Yang, Z. Fu, Y. Yang, ZhWu. Ch Zhang, T.Q. Sheng, J. Am. Ceram. Soc. **98**, 2595–2600 (2015)
36. F. Huang, Y. Gao, J.C. Zhou, J. Xu, Y.S. Wang, J. Alloys Compd. **639**, 325–329 (2015)
37. B. Dong, D. Liu, X. Wang, T. Yang, S. Miao, C. Li, Appl. Phys. Lett. **90**, 181117 (2007)
38. S.K. Singh, K. Kumar, S.B. Rai, Sens. Actuators, A **149**, 16–20 (2009)
39. S. Zhou, K. Deng, X. Wei, G. Jiang, C. Duan, Y. Chen, M. Yin, Opt. Commun. **291**, 138–142 (2013)
40. G. Liu, L. Fu, Z. Gao, X. Yang, Z. Fu, Z. Wang, Y. Yang, RSC Adv. **5**(2015), 51820–51825 (1827)
41. A. Pandey, V.K. Rai, V. Kumar et al., Sens. Actuators B Chem **209**, 352–358 (2015)
42. J. Cao, F. Hu, L. Chen, H. Guo, C. Duan, M. Yin, J. Am. Ceram. Soc. **100**, 2108–2115 (2017)
43. X. Liu, R. Lei, F. Huang, D. Deng, H. Wang, S. Zhao, S. Xu, J. Lumin. **210**, 119–127 (2019)
44. G. Xiang, X. Liu, W. Liu, B. Wang, Z. Liu et al., J. Am. Ceram. Soc. **103**, 2540–2547 (2020)
45. T. Zheng, L. Zhou, X. Qiu, D. Yang, M. Runowski et al., J. Lumin. **227**, 117517 (2020)
46. Z. Li, Q. Han, T. Yan, Z. Huang, Y. Song, Y. Wang, X. Zhang, J. Alloys Compd. **904**, 164009 (2022)
47. W. Zheng, B. Sun, Y. Li, R. Wang, A.C.S. Appl, Nano Mater. **4**, 3922–3931 (2021)
48. B. Cao, J. Wu, X. Wang, Y. He, Z. Feng, B. Dong, Sensors **15**, 30981–30990 (2015)